

Emergent correlations in the selected link-times along optimal paths

Iván Álvarez Domenech,¹ Javier Rodríguez-Laguna,² Pedro Córdoba-Torres,¹ and Silvia N. Santalla³

¹*Dpto. Física Matemática y de Fluidos, Universidad Nacional de Educación a Distancia (UNED), Madrid (Spain)*

²*Dpto. Física Fundamental, Universidad Nacional de Educación a Distancia (UNED), Madrid (Spain)*

³*Dpto. Física & GISC, Universidad Carlos III de Madrid, Leganés (Spain)*

(Dated: January 24, 2026)

In the context of first-passage percolation (FPP), we investigate the statistical properties of the *selected link-times* (SLTs) –the random link times comprising the optimal paths (or geodesics) connecting two given points. We focus on weakly disordered square lattices, whose geodesics are known to fall under the Kardar-Parisi-Zhang (KPZ) universality class. Our analysis reveals universal power-law decays with the end-to-end distance for both the average and standard deviation of the SLTs, along with an intricate pattern of long-range correlations, whose scaling exponents are directly linked to KPZ universality. Crucially, the SLT distributions for diagonal and axial paths exhibit significant differences, which we trace back to the distinct directed and undirected nature, respectively, of the underlying geodesics. Moreover, we demonstrate that the SLT distribution violates the conditions of the central limit theorem. Instead, SLT sums follow the Tracy-Widom distribution characteristic of the KPZ class, which we associate with evidence for the emergence of high-order long-range correlations in the ensemble.

I. INTRODUCTION

Selection and conditioning often induce correlations in otherwise independent and identically distributed (iid) random variables. Simple examples include the Brownian bridge, i.e. random walks constrained to start and end at the same points [1], and order statistics, i.e. sorted iid variates [2]. In both cases, emergent long-range correlations among random variables appear as a result of either a global constraint or a sorting procedure. Another counterintuitive effect is known as *collider bias* or Berkson's paradox, i.e. selecting individuals above a certain threshold for the sum of different uncorrelated traits induces a spurious correlation between them [3–5]. This explains the existence of unexpected negative correlations between luminosity and distance in flux-limited astronomical catalogs (Malmquist bias) [6], or the apparent ties between independent lifetimes in risk assessment [7]. Finally, in quantitative genetics, evolutionary selection of a trait which is the sum of several effects associated to independent loci tends to reduce its variance through the emergence of negative correlations among them, which is known as Bulmer effect [8]. Our starting hypothesis is that such emergent correlations must also appear among the link-times which are actually selected by geodesics in random media –also known as optimal paths–, even though the whole ensemble of link-times remains uncorrelated.

The characterization of *optimal paths* in disordered networks [9, 10], also known as *first-passage percolation* (FPP) [11, 12], is deeply connected to other relevant systems in statistical mechanics, such as geodesics in random metrics [13, 14], minimum spanning trees [15–19], directed polymers in random media [20], and percolation models [21]. Moreover, it is also crucial for several applications involving random media, including transport in communication networks [16–19, 22, 23], fluid or current flow [24–30], magnetotransport [31, 32], epidemic spread

ing [33], and fracture [34]. Specifically, we will consider the FPP model on square lattices for which the crossing times associated to the edges, or *link times* (LTs), are weakly disordered iid random variables [35]. Interestingly, the statistical properties of geodesics between two given points fall within the 1+1D Kardar-Parisi-Zhang (KPZ) universality class [36, 37], which first appeared in the analysis of growing interfaces [38, 39], but which has since found applications in numerous areas of physics and mathematics [40]. Indeed, the fluctuations in the arrival time T of a geodesic spanning a Euclidean distance d are known to scale as $\sigma_T \sim d^\beta$, where $\beta = 1/3$ is the growth exponent of KPZ, while its average lateral deviation from the straight line scales as $h \sim d^{1/z}$, where $z = 3/2$ is the dynamic exponent [36]. Moreover, systems within the KPZ class tend to present universal local fluctuations, corresponding to one of the probability distributions in the Tracy-Widom (TW) family [40]. We have recently shown [37] that the local fluctuations of the isochrones follow the TW distribution associated with the Gaussian unitary ensemble (TW-GUE), and there is evidence that the latter could also govern the arrival time fluctuations [36]. Finally, let us stress that the geodesic length ℓ is proportional to the end-to-end distance d in all the considered cases.

In this work we aim to characterize the ensemble of *selected link-times* (SLTs), i.e., the LTs which are actually chosen by optimal paths spanning different Euclidean distances, in the weak disorder regime. Naturally, we expect the SLTs to take lower values than those of the whole ensemble of LTs, but *how much lower?* The reduction is expected to be smaller near the geodesic ends –because of the small number of choices– than in the geodesic bulk. Crucially, the sum of the SLTs along a geodesic corresponds to the total arrival time, which presents non-Gaussian statistics. Therefore, the SLTs must violate the hypotheses of the central limit theorem (CLT) [41–43]. Such violation, as we will see, takes place

through the emergence of long-range non-Wick correlations of higher order [44, 45], which we will associate to KPZ scaling using an Ansatz inspired in 2D conformal field theory (CFT) [46]. This way, we will make contact with the area of *full-counting statistics* (FCS) [47–49], in which integrals of a certain physical density (energy, magnetization, etc.) subject to random fluctuations with high-order long-range correlations are shown to evade the constraints of the CLT.

This article is organized as follows. Section II describes the basic properties of our physical model. The global probability distribution of the SLTs is discussed in Sec. III, while Sec. IV characterizes the dependence on the position along the geodesic and the link direction. Section V discusses the emergent correlations among the SLTs, both for two-point and higher-order correlators, which are required to violate the conditions of the CLT and give rise to the TW distribution of the arrival times. The article ends with a summary of our conclusions and proposals for further work.

II. MODEL

Let us consider the square lattice \mathbb{Z}^2 , whose edge set is denoted by \mathcal{E} . We associate to each edge $e \in \mathcal{E}$ an LT $t_e > 0$, which are. The set of LTs are iid random variables with common probability distribution $F(t)$ ($F(0) = 0$), probability density function (pdf) $f(t)$, mean τ , and deviation σ . A path γ of length $\ell = |\gamma|$ is defined as a sequence of edges $\gamma = \{e_i\}_{i=1}^\ell$ such that e_i and e_{i+1} share only one endpoint. The crossing time associated to the path is given by $T(\gamma) = \sum_{e \in \gamma} t_e$. Now, given two nodes $\mathbf{x}, \mathbf{y} \in \mathbb{Z}^2$, we may consider the path joining them presenting the minimum crossing time, that is, the path γ_{opt} such that

$$T(\gamma_{\text{opt}}) = \min_{\gamma \in \Gamma(\mathbf{x}, \mathbf{y})} T(\gamma), \quad (1)$$

where $\Gamma(\mathbf{x}, \mathbf{y})$ is the set of paths joining \mathbf{x} with \mathbf{y} . This path γ_{opt} is called the *geodesic* or *optimal path* between \mathbf{x} and \mathbf{y} , and the minimum crossing time associated is called the *arrival time* between the two nodes, denoted as $T(\mathbf{x}, \mathbf{y}) \equiv T(\gamma_{\text{opt}})$. For notational convenience, we will set the initial node of all our geodesics at the origin of coordinates, $\mathbf{x} = 0$, and denote $T(\mathbf{x}) \equiv T(0, \mathbf{x})$. We may define now the ball at time $t > 0$ around the origin, $B(t)$, as

$$B(t) = \{\mathbf{x} \in \mathbb{Z}^2 : T(\mathbf{x}) \leq t\}. \quad (2)$$

The boundary of $B(t)$, $\partial B(t)$, will be called the *isochrone* correponding to time t .

When the disorder is weak, the coefficient of variation of the LT distribution, $\text{CV} \equiv \sigma/\tau$, plays a central role in the statistical properties of our system [36]. For

$\text{CV} \ll 1$, the isochrones converge towards a diamondlike limit shape that reflects the geometry of the underlying lattice [37]. Yet, as the CV increases, the diamond transforms continuously into a circumference, and we observe isotropic growth. As it was mentioned earlier, the deviation of the arrival times between points separated a large distance d grows as $\sigma_T(d) \sim d^\beta$, where $\beta = 1/3$ is the growth exponent of KPZ. Along a diagonal, this asymptotic behavior takes place for all d , but along an axis, the deviation initially grows as $\sigma_T(d) \sim d^{1/2}$, up to a certain crossover distance, $d_c \equiv \tau^2/(3\sigma^2)$. The difference between both cases is that the geodesic along the axis is non-degenerate in the homogeneous case, i.e. when all the LTs are equal [36]. Moreover, the average lateral deviation between the geodesic and the straight line joining the endpoints, h , scales as $h \sim d^{1/z}$ for large d , where $z = 3/2$ is the dynamic exponent of KPZ. Yet, if the points lie along an axis, the lateral deviation is negligible for $d \ll d_c$ [36].

In this work we have characterized the statistical properties of the SLTs in geodesics both along the axial and diagonal directions on a $(2L+1) \times (2L+1)$ square lattice with $L = 1005$. Two different LT distribution families have been employed to that end. On the one hand, the uniform distribution on the interval $[a, b]$, for which the maximal attainable value of the CV is $1/\sqrt{3} \approx 0.57$, since $a \geq 0$ necessarily. On the other hand, we have used the Weibull distribution, given by the probability density function

$$f(t) = \frac{k}{\lambda} \left(\frac{t}{\lambda} \right)^{k-1} \exp \left(-(t/\lambda)^k \right), \quad (3)$$

which allows for any positive value of the CV.

In all our simulations, we fix the mean value of the LT distribution, $\tau = 5$, and choose different values of the CV in order to survey the different observables. Thus, we use the notation $\text{U}(\text{CV})$ and $\text{Wei}(\text{CV})$ respectively for the uniform and Weibull distributions with parameter CV. Also, to perform our statistical analysis we employ $N_s = 2 \cdot 10^4$ different noise realizations. Finally, the maximum end-to-end distance considered here will be $d_{\text{max}} = 1000$ for the axis and $d_{\text{max}} = 1000\sqrt{2}$ for the diagonal.

III. GLOBAL SLT DISTRIBUTION

Geodesics tend to pass through links with low crossing times, i.e. the SLTs tend to be lower than the original LTs, and in this section we characterize the difference between both distributions. We will denote by $\hat{f}(t)$ the *global* pdf for the SLTs along the different geodesics, and we will extend the notation to the global probability function $\hat{F}(t)$, and to the mean and standard deviation, $\hat{\tau}$ and $\hat{\sigma}$, respectively.

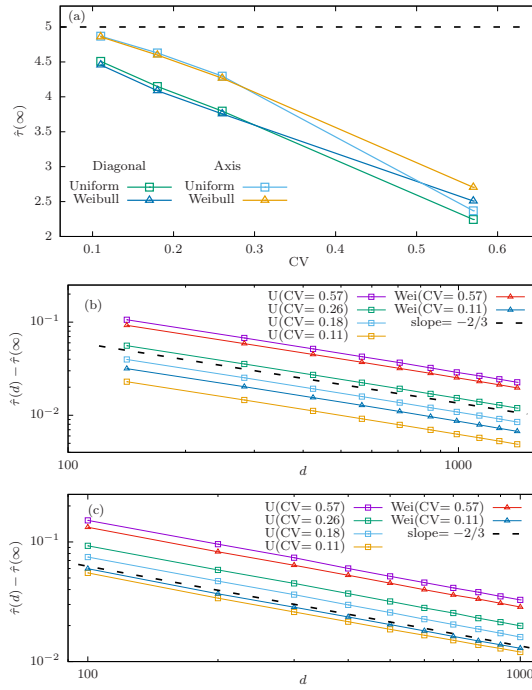


Figure 1. (a) Asymptotic value of the global SLT mean as function of the CV for the two distributions and the two lattice directions. The broken line indicates the LT mean. (b) Convergence of the SLT averages towards their asymptotic values for geodesics along the diagonal, as we increase the end-to-end distance d . (c) Same data, along the axis. The broken line in both panels represents power-law behavior with exponent $-1/z$.

A. Mean and deviation of the global SLT distribution

In this section we will consider the dependence of the first two moments of the global SLT distribution on the end-to-end distance d , i.e. $\hat{\tau}(d)$ and $\hat{\sigma}(d)$, for different values of the CV. Naturally, we always have $\hat{\tau}(d) \leq \tau$, and in all the considered cases we observe a steady decay of $\hat{\tau}(d)$ as d increases, approaching a limit value $\hat{\tau}(\infty)$ as $d \rightarrow \infty$, which is consistent with the results of the limit-shape theorem [50, 51]. Those limiting values are shown for both distributions in Fig. 1 (a), along the axis and the diagonal. We observe in all cases that $\hat{\tau}(\infty)$ decreases as the CV increases. For low values of the CV, the shift with respect to the mean LT (broken line) is always lower along the axis than for the diagonal. Yet, that anisotropy seems to disappear for strong disorder.

It is therefore relevant to consider how $\hat{\tau}(d)$ decays with the distance d towards their asymptotic values, $\hat{\tau}(\infty)$, which is shown in Fig. 1 (b) for the diagonal and in Fig. 1 (c) for the axis. In all those cases we observe a well-defined power-law decay,

$$\hat{\tau}(d) - \hat{\tau}(\infty) \sim d^{-\alpha_\tau}, \quad (4)$$

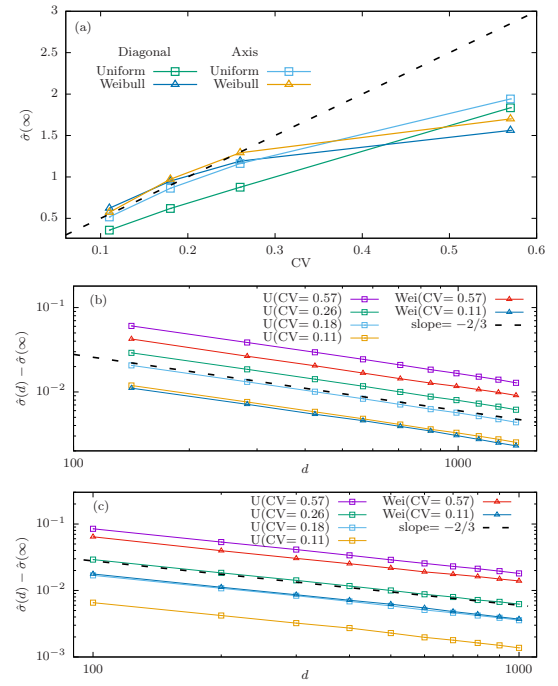


Figure 2. (a) Asymptotic value of the global SLT deviation as function of the CV for the two distributions and the two lattice directions. The broken line indicates the LT deviation. (b) Convergence of the SLT deviations towards their asymptotic values for geodesics along the diagonal, as we increase the distance d . (c) Same data, along the axis. The broken line in both panels represents power-law behavior with exponent $-1/z$.

where $\alpha_\tau \approx 2/3$ (broken line).

It is possible to provide a heuristic argument in order to understand this behavior. The expected value of the minimum of n iid random variables extracted from a probability distribution with a bounded support $[a, b]$ converges to a –under very mild conditions– as n^{-1} , while its deviation decreases also as n^{-1} [2]. In our case, since the geodesic tends to explore a lateral deviation of order $h \sim d^{2/3}$, it is reasonable to expect the aforementioned scaling regime. Indeed, this is the observed behavior for all the considered distributions.

Similarly, we may compute the global SLT deviation $\hat{\sigma}(d)$ as a function of the distance d for the same set of geodesics. We also obtain a decay towards an asymptotic value $\hat{\sigma}(\infty)$, which need not be lower than σ . Indeed, Fig. 2 (a) shows that for low values of the CV we may have $\hat{\sigma}(\infty) > \sigma$. Still, these SLT deviations converge towards their asymptotic values following a power-law with the same exponent as the mean,

$$\hat{\sigma}(d) - \hat{\sigma}(\infty) \sim d^{-\alpha_\sigma}, \quad (5)$$

with $\alpha_\sigma \approx \alpha_\tau \approx 2/3$, as we can see in Fig. 2 (b) for the diagonal and Fig. 2 (c) for the axis.

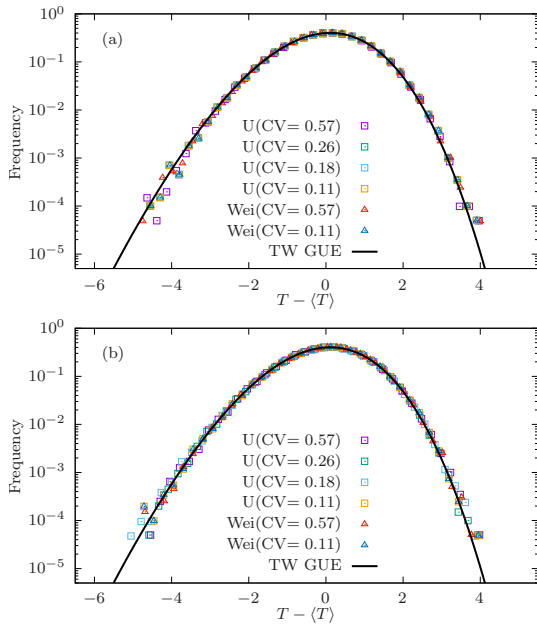


Figure 3. Histograms of χ , defined in Eq. (6), which is a standardized version of the arrival time T , for the maximum spanning distance d_{\max} along (a) the diagonal and (b) the axis, and different LT distributions. The suitably rescaled and reversed TW-GUE distribution is shown for comparison.

B. Distribution of the SLT sum

The SLTs are chosen to minimize the arrival time. If the SLTs were selected through independent random sampling of the original LT distribution, we would expect the Central Limit Theorem (CLT) to apply. In that case, arrival time deviations between points separated by a large distance d would scale as $\sigma_T(d) \sim d^{1/2}$ with normal asymptotic fluctuations. However, we observe a scaling with the KPZ exponent $\beta = 1/3$ and values of the skewness and kurtosis that differ from those associated with the Gaussian distribution [36].

In order to fully determine the nature of the arrival time fluctuations, let us consider a standardized variable,

$$\chi \equiv \frac{T - \langle T \rangle}{\sigma_T}. \quad (6)$$

and construct the histograms of this variable χ for geodesics across a distance d_{\max} for different LT distributions. The results are shown in Fig. 3 for (a) the diagonal direction and (b) the axis. We observe an extremely good fit to a suitably standardized TW-GUE distribution, which has been reversed along the horizontal axis because χ exhibits negative skewness, unlike the radial fluctuations of the isochrones [37].

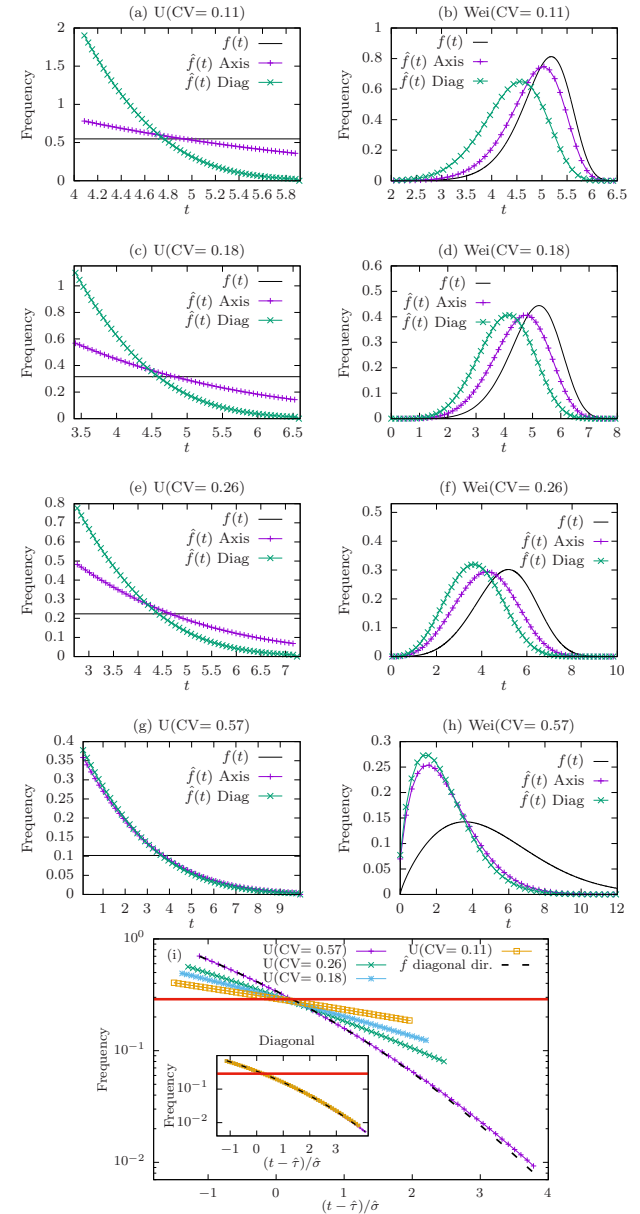


Figure 4. (a)-(h) SLT histograms, $\hat{f}(t)$, for geodesics reaching the maximum distance d_{\max} along the axis and the diagonal, using different LT distributions, along with the original LT probability density $f(t)$. Left and right columns show uniform and Weibull cases respectively, with CV growing from top to bottom. (i) Standardized SLT histograms for the uniform distribution along the axis and the diagonal (inset) directions, the horizontal line representing the original LT distribution. For the sake of comparison, we have displayed in the main figure (axis), the curve of the inset (diagonal) corresponding to $\text{CV}=0.57$.

C. Global properties of the SLT distribution

The mean and deviation of the selected times do not inform us about the changes in shape between the LT and the global SLT distribution. Figures 4 (a) to (h)

compare the corresponding histograms for geodesics spanning the maximum distance d_{\max} both along the axis and the diagonal, and different LT distributions. On the left we observe the results for the uniform distribution, and on the right the Weibull case, while the CV increases from top to bottom. In each case, the corresponding original LT density function $f(t)$ has been displayed by a continuous line. Notice that in all cases the SLT histogram *shifts leftwards*, towards lower times. Yet, the shift is always lower along the axis than on the diagonal, even though both tend to become similar as the CV increases. This result agrees with the behavior of $\hat{\tau}(\infty)$ displayed in Fig. 1 (a). Figure 4 (i) shows all the SLT distributions for the uniform case, after a standardization procedure, so that all of them have zero mean and variance one. Notice that all standardized histograms coincide approximately for the diagonal (inset), while they converge towards the diagonal shape for the axis (main panel), as the CV increases.

Can we make the idea of similarity and convergence between the SLT distributions more precise? Certainly, by making use of the *Kolmogorov-Smirnov* (KS) distance between two probability distributions, $F(t)$ and $\hat{F}(t)$, defined as

$$D_{\text{KS}}(\hat{F}(t) \| F(t)) = \sup_t |\hat{F}(t) - F(t)|. \quad (7)$$

The KS distance between the LT and SLT distributions can be interpreted as the degree of optimization achieved along the geodesic. Concretely, if we have a single t^* such that $f(t^*) = \hat{f}(t^*)$, then the KS distance can be understood as the amount of probability that shifts from values above t^* to those below t^* , see Fig. 5 (a) for an illustration.

Figure 5 (b) shows the KS distances between the LT and the SLT distributions in the asymptotic regime, for $d \rightarrow \infty$. Notice that, along the axis, the KS distance between both distributions grows quickly with the CV, in a similar way for the uniform and the Weibull distributions. Yet, along the diagonal, the asymptotic KS distance remains nearly constant for all the levels of disorder.

It is also interesting to observe how the KS distance between the LT and the SLT distributions approaches its asymptotic value as the distance d increases, which is shown in Fig. 5 for the diagonal (c) and the axis (d) directions. In all cases we observe a power-law approach,

$$|D_{\text{KS}}(d) - D_{\text{KS}}(\infty)| \sim d^{-\alpha_{\text{KS}}}, \quad (8)$$

with $\alpha_{\text{KS}} \approx 2/3$, as it was the case for the mean and deviation.

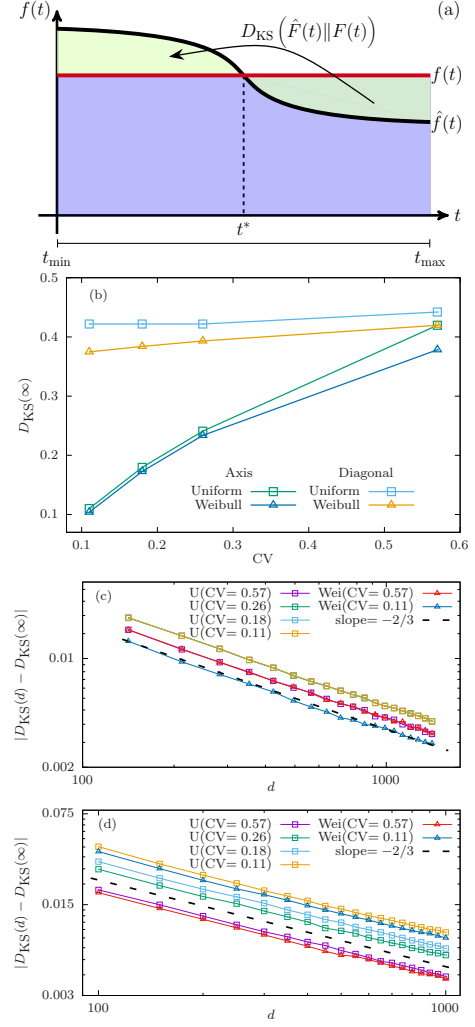


Figure 5. (a) Schematic representation of the probability shift between the SLT distribution (solid line) and the original LT distribution (horizontal red line). (b) KS distance between the LT and the SLT distributions for asymptotically large distances along the axis and the diagonal, as a function of the CV for the two LT distributions. (c) Convergence of the KS distances between the LT and the SLT distributions toward their asymptotic values as a function of the distance for the diagonal direction. (d) Same data, for the axis. The broken line in both panels represents power-law behavior with exponent $-1/z$.

IV. LOCAL SLT DISTRIBUTION

A. Local mean and deviation

Geodesics are specially constrained near their extremes. Therefore, it is reasonable to consider how the SLT distribution for a given link depends on its relative position along the geodesic. Let p denote the distance to the closest extreme, and let $\hat{f}_p(t)$ denote the *local* SLT distribution at that position, with $\hat{\tau}_p$ and $\hat{\sigma}_p$ standing for the corresponding mean and deviation. Thus, we expect

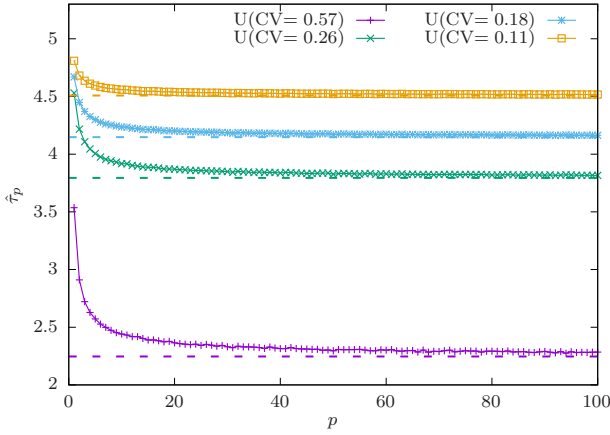


Figure 6. Average value of the local SLTs, $\hat{\tau}_p$, as a function of the distance to the closest extreme, p , for geodesics reaching the maximum distance d_{\max} along the diagonal and a uniform distribution with different CV. The horizontal lines denote the corresponding values of the global SLT mean, $\hat{\tau}$. Note that, in all cases, the LT mean is $\tau = 5$.

$\hat{\tau}_1$ to be close to τ since there are only four options to choose the first edge. Nonetheless, as we increase p , we expect $\hat{\tau}_p$ to decrease further, and to eventually approach the global value $\hat{\tau}$. Figure 6 shows the expected value $\hat{\tau}_p$ as a function of p for geodesics to distance d_{\max} along the diagonal and different values of the CV of the uniform distribution. The horizontal lines denote the global values $\hat{\tau}$, and we observe how $\hat{\tau}_p$ converges towards them.

We may now ask about the convergence of the local mean $\hat{\tau}_p$ towards the global mean $\hat{\tau}$ for different distributions and directions, as a function of the distance p to the closest extreme. The results are shown in Fig. 7 (a) for the diagonal and in Fig. 7 (b) for the axis, in logarithmic scale, in order to highlight the power-law decay,

$$\hat{\tau}_p - \hat{\tau} \sim p^{-\alpha_p}. \quad (9)$$

We observe that, along the diagonal, $\alpha_p \approx 2/3$ for all the considered distributions. Indeed, this result may be accounted for using a similar heuristic argument as that provided in Sec. III for the decay of $\hat{\tau}(d)$ with the distance. Yet, along the axial direction, the data suggest a faster decay, with $\alpha_p \approx 1$, see Fig. 7 (b). Local deviations, $\hat{\sigma}_p$, also approach their global value $\hat{\sigma}$ as a power law, as we can check in Fig. 7 (c) for the diagonal and in Fig. 7 (d) for the axis, with similar scaling exponents.

Finally, it is worth noting that the constraints near the endpoints do not affect the statistics of the arrival time fluctuations. Although not shown here, we obtained the histograms of the sum of the SLTs belonging to the bulk of the geodesic, thus discarding the SLTs near the endpoints. To do this, we considered only the SLTs that satisfy $|t_p - \hat{\tau}| < \delta$, for various values of δ . In all cases, we obtained the TW-GUE distribution.

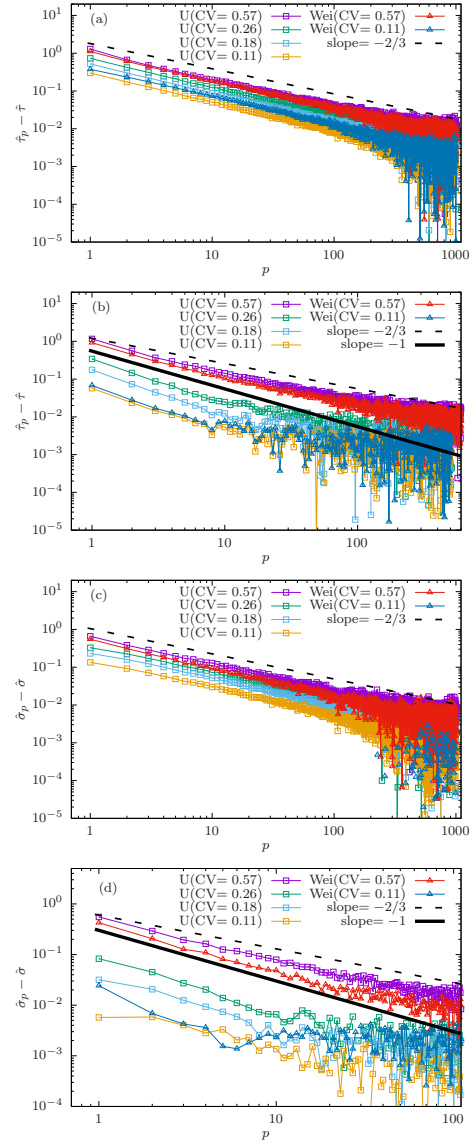


Figure 7. Average local SLT excess, $\hat{\tau}_p - \hat{\tau}$, for a link at a distance p from the closest extreme of geodesics reaching the maximum distance d_{\max} along (a) the diagonal and (b) the axis, for several uniform and Weibull distributions. Local SLT excess deviation, $\hat{\sigma}_p - \hat{\sigma}$, for the same distributions, along the diagonal (c) and the axial (d) directions. Broken and solid lines represent power-law behaviors with exponents $-1/z$ and -1 , respectively.

B. Directional effects

Let us consider geodesics along an axial direction. In this case we may distinguish between *longitudinal* and *transverse links*, depending on whether they point along the axis or in the perpendicular direction. Transverse links always increase the geodesic length and, therefore, we expect the associated SLTs to take specially low values. Let $\hat{f}_{\parallel}(t)$ and $\hat{f}_{\perp}(t)$ denote their respective pdfs. Furthermore, we will label the longitudinal links accord-

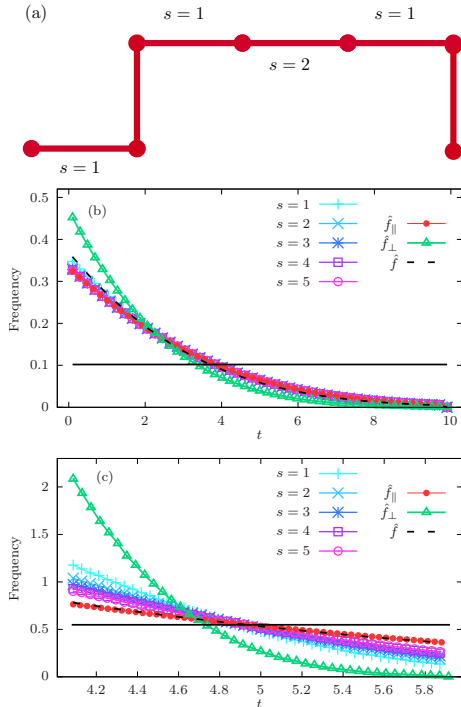


Figure 8. (a) A schematic representation of the label s for longitudinal links along an axial geodesic. (b) and (c) Histograms of the longitudinal and transverse SLTs, \hat{f}_{\parallel} and \hat{f}_{\perp} , for a uniform disorder with $\text{CV}=0.57$ (b) and $\text{CV}=0.11$ (c), along with the histograms of longitudinal SLTs for different values of s , $\hat{f}_{\parallel,s}$. Corresponding global SLT histogram and original LT pdf have been displayed in both panels by the broken line and the solid black line, respectively, in order to compare. Results correspond to geodesics spanning the maximum distance d_{\max} along the axis.

ing to the distance s to the closest transverse link along the geodesic, as illustrated in Fig. 8 (a).

Figure 8 shows different SLT histograms for both transverse and longitudinal selected-links for (b) a noisy uniform distribution with $\text{CV}=0.57$ and (c) a low-noise uniform distribution with $\text{CV}=0.11$. In each panel, we display the histograms of: all SLTs, \hat{f} , the transverse SLTs, \hat{f}_{\perp} , the longitudinal SLTs, \hat{f}_{\parallel} , and the longitudinal SLTs with different values of s , $\hat{f}_{\parallel,s}$. Transverse SLTs always take lower values, as expected, and their histogram is close to the global SLT histogram along the diagonal (not shown here). Longitudinal SLTs, on the other hand, are closer to the original LT distribution (horizontal line) in the low disorder case, Fig. 8 (c), and in this case they show an interesting dependence on the distance to the closest transverse link, s . Indeed, we observe that longitudinal SLTs take lower values for $s = 1$, and approach the global longitudinal histogram as s increases.

V. CORRELATIONS ALONG THE SLT

Once we have characterized the global properties of the SLT distribution in Sec. III, and the local properties in Sec. IV, it is now the turn of their *correlation structure*. Despite the fact that the original LTs are iid random variates, we are aware that selection and conditioning may induce an intricate pattern of correlations among them, as illustrated e.g. in Berkson's paradox [3–5].

Theoretical arguments strongly suggest the emergence of long-range correlations along the SLT distribution. Arrival times are sums of SLTs, and their deviation scales as d^{β} , where $\beta = 1/3$ is the growth exponent of KPZ. Furthermore, the probability distribution for the arrival times, suitably rescaled, corresponds to the Tracy-Widom distribution for the GUE ensemble. These two well known facts would be impossible if the SLTs were independent random variables. Indeed, the CLT would ensure in this case that the arrival times should be Gaussian, and their deviation should scale as $d^{1/2}$. As we will see at the end of this section, such a strong violation of the hypotheses of the CLT imposes very strict conditions on the correlations among the SLTs.

A. Two-point correlations

Let us define $\bar{t}_p \equiv \hat{t}_p - \hat{\tau}_p$, so that the covariance between SLTs located at positions p and q along the geodesic becomes

$$\text{Cov}(p, q) \equiv \langle \bar{t}_p \bar{t}_q \rangle. \quad (10)$$

The (two-point) correlation between them is then defined as

$$C(p, q) \equiv \frac{\text{Cov}(p, q)}{\hat{\sigma}_p \hat{\sigma}_q}. \quad (11)$$

Furthermore, if we expect a translationally invariant structure we may define the correlation function as a spatial average,

$$C(k) \equiv \overline{C(p, p+k)}. \quad (12)$$

Naturally, we are aware that the SLTs do not constitute a translationally invariant random process. Yet, a *bulk* regime is achieved in the central part of large geodesics.

Figure 9 shows the the absolute value of the correlation function $C(k)$ for geodesics spanning the maximum distance d_{\max} along the diagonal, and different disorder distributions. The correlation function $C(k)$ is always *negative* in this case (see inset), because selecting a specially low link-time may force us to pay some price in the neighboring link times, which tend to be slightly larger than their mean. We also observe that correlations decay as a power-law with a common scaling exponent,

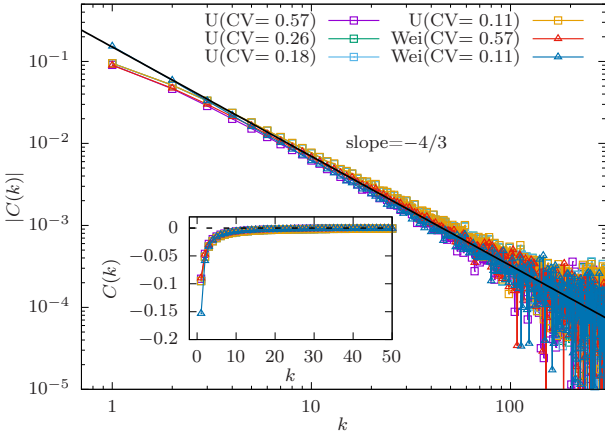


Figure 9. Correlation function $C(k)$ for geodesics reaching the maximum distance d_{\max} along the diagonal and different disorder distributions. The main panel shows the log-log plot of the absolute value, while the inset displays the bare values in linear scale. The solid line represents power-law behavior with exponent $-4/3$.

$$C(k) \sim k^{-\gamma}, \quad (13)$$

with $\gamma = 4/3$, which we can associate to the KPZ universality class. Indeed, the variance of the arrival times can be computed as

$$\sigma_T^2 = \langle T^2 \rangle - \langle T \rangle^2 = \sum_{p,q} C(p,q) \sim d^{2-\gamma}, \quad (14)$$

where we have made use of the fact that $\ell \propto d$ in the weak disorder regime. Since KPZ scaling demands that $\sigma_T^2 \sim d^{2\beta}$, we deduce that $\gamma = 2 - 2\beta = 4/3$. In other words: *the correlation scaling exponent along the SLTs can be readily linked to the KPZ class*.

Figure 10 (a) shows the correlation function, $C(k)$, along the axis, for several disorder distributions and for geodesics reaching the maximum distance d_{\max} . For the higher disorder case ($CV = 0.57$), we observe that the correlation function $C(k)$ tends to zero as a power law with the same exponent obtained along the diagonal. However, the sign of the correlation function behaves in a surprising way for low disorder ($CV = 0.11$), since $C(k) < 0$ for very small k , but then jumps to a large positive value, from which it decays to zero.

In order to understand the complex pattern displayed by the correlation function along the axis, we should consider their *directional information*. In Sec. IV we distinguished between longitudinal and transverse links, and we may make a similar distinction here. Given a geodesic, let us consider the terms of the form $\pi(p, q) \equiv \bar{t}_p \bar{t}_q / \hat{\sigma}_p \hat{\sigma}_q$ which involve different combinations of link types. We may distinguish three such combinations:

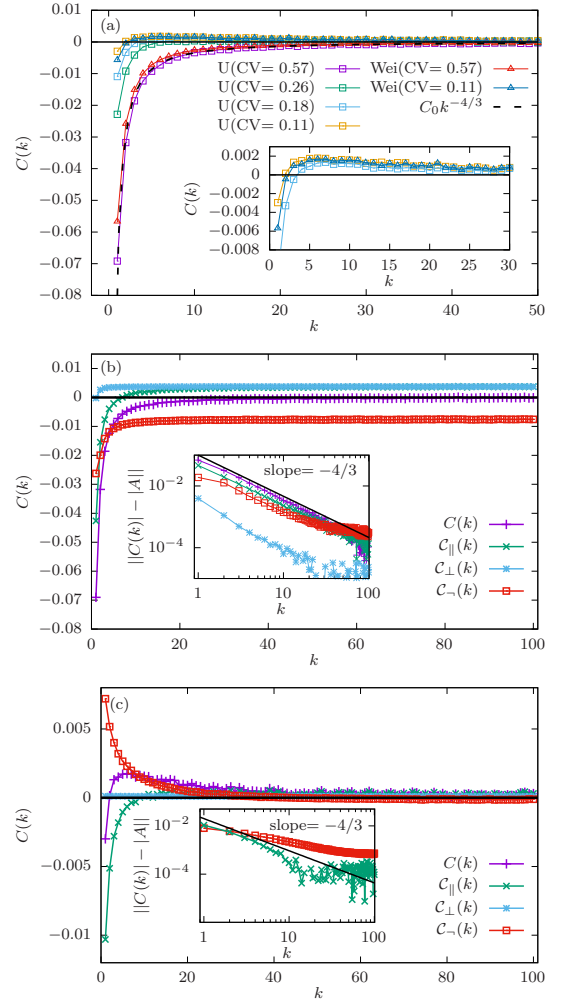


Figure 10. (a) Correlation function, $C(k)$, for geodesics reaching the maximum distance d_{\max} along the axis and different disorder distributions. A power law with exponent $-4/3$, obtained by fitting the correlation function for the higher-disorder case ($CV=0.57$), is also shown. The inset shows a zoom of the positive values. (b)-(c) Correlation function, $C(k)$, and its directional contributions, $C_{\parallel}(k)$, $C_{\perp}(k)$ and $C_{-}(k)$, for geodesics reaching the maximum distance d_{\max} along the axis and a uniform distribution with (b) $CV=0.57$ and (c) $CV=0.11$. Insets show their convergence towards their asymptotic values, represented by A .

- Longitudinal contribution, $\pi_{\parallel}(p, q)$, if both p and q are longitudinal links.
- Transverse contribution, $\pi_{\perp}(p, q)$, if both p and q are transverse links.
- Mixed contribution, $\pi_{-}(p, q)$, if one of them is longitudinal and the other is transverse.

Then, we perform the average over all products of the same type within each geodesic as a function of $k = p - q$, to obtain the following decomposition of the correlation

function:

$$C(k) = \underbrace{\overline{\langle \mathcal{C}_{\parallel}(k) \rangle}}_{\mathcal{C}_{\parallel}(k)} + \underbrace{\overline{\langle \mathcal{C}_{\perp}(k) \rangle}}_{\mathcal{C}_{\perp}(k)} + \underbrace{\overline{\langle \mathcal{C}_{\neg}(k) \rangle}}_{\mathcal{C}_{\neg}(k)}, \quad (15)$$

where the overline indicates the appropriate average over products of the same type within each geodesic.

Let us now return to Fig. 10, and observe the behavior of the directional contributions to the correlation functions. For high CV, see Fig. 10 (b), all three contributions grow monotonously. The longitudinal term $\mathcal{C}_{\parallel}(k)$ starts out negative for very low k , but finally converges to a positive value for large k . The transverse term, $\mathcal{C}_{\perp}(k)$, is always positive, and the mixed term remains negative. The inset shows their convergence towards their asymptotic value, and we can see that their behaviors are compatible with the global expected scaling. Noticeably, the three contributions approach asymptotically a nonzero value. To understand this behavior, let us recall that the average of the SLTs at positions p and q are obtained without taking into account the link direction at those positions. If we denote by $\hat{\tau}_{\perp}$ and $\hat{\tau}_{\parallel}$ the mean values of the transverse and longitudinal SLTs, respectively, we can deduce from Fig. 8 the following inequalities:

$$\hat{\tau}_{\perp} \leq \hat{\tau} \leq \hat{\tau}_{\parallel}, \quad (16)$$

where equality holds in the case $\hat{f}_{\perp} = \hat{f}_{\parallel}$. Indeed, the sign of the asymptotic values of each contribution is primarily determined by the inequalities in Eq. (16). In the case of the transverse contribution, $\mathcal{C}_{\perp}(k)$, we have $\hat{\tau}_{\perp} - \hat{\tau} < 0$, and the sign of its asymptotic value is given by the sign of the product $(\hat{\tau}_{\perp} - \hat{\tau})(\hat{\tau}_{\perp} - \hat{\tau}) > 0$. On the other hand, for the longitudinal contribution, $\mathcal{C}_{\parallel}(k)$, we have $\hat{\tau}_{\parallel} - \hat{\tau} > 0$, and thus $(\hat{\tau}_{\parallel} - \hat{\tau})(\hat{\tau}_{\parallel} - \hat{\tau}) > 0$. For the mixed contribution, $\mathcal{C}_{\neg}(k)$, the cross product $(\hat{\tau}_{\parallel} - \hat{\tau})(\hat{\tau}_{\perp} - \hat{\tau})$ is negative, thus explaining the sign of all contributions.

Finally, Fig. 10 (c) shows the same data for a low disorder uniform distribution with CV=0.11. The longitudinal term is positive and grows monotonously, as in the high-disorder case displayed in Fig. 10 (b), and the transverse term is almost negligible. Remarkably, the mixed contribution is now positive and decays monotonously. These behaviors provide a route to explain the complex behavior of the final correlator. To understand these patterns, we need to draw attention to the fact that, for weak disorder, the number of transverse SLTs is much smaller than the number of longitudinal SLTs, and two consecutive transverse SLTs constitute an event of negligible probability. Consequently, the value of the local mean $\hat{\tau}_p$ is close to the mean associated with longitudinal SLTs, $\hat{\tau}_{\parallel}$, resulting in a small positive asymptotic value for \mathcal{C}_{\parallel} . In addition, the relatively small number of

transverse links explains the low value of the transverse contribution \mathcal{C}_{\perp} . To explain the behavior of the mixed contribution, $\mathcal{C}_{\neg}(k)$, we recall the results displayed in Fig. 8 (b), which showed that longitudinal links tend to have lower values as they approach the closest transverse link. If we denote by $\hat{\tau}_{\parallel,s}$ the mean value of the longitudinal SLTs at a distance s from the closest transverse link, we have that the mixed contribution is governed by terms of the form $(\hat{\tau}_{\parallel,s} - \hat{\tau})(\hat{\tau}_{\perp} - \hat{\tau})$, which are positive for small values of k . As k increases, $\hat{\tau}_{\parallel,s}$ approaches $\hat{\tau}$, thus yielding the monotonically decreasing behavior of the contribution $\mathcal{C}_{\neg}(k)$.

B. High-order correlations and the violation of the CLT hypotheses

Yet, long-range two-point correlations need not lead to a violation of the hypotheses of the CLT [41–43], which in this case is ruled by the Breuer-Major theorem [44, 45]. In intuitive terms, if the two-point correlation fulfills some mild conditions, we may perform a Cholesky decomposition of the covariance matrix, and express the SLT vector as a linear transformation of another vector of iid random variates, for which the CLT holds. Therefore, our previous results do not explain by themselves the emergence of a strongly non-Gaussian limit distribution for the SLT sums, i.e. the Tracy-Widom distribution, which is not even infinitely divisible [52].

Indeed, in order to ensure Gaussianity of the sum of n correlated variables $\{X_i\}$ with zero average and finite covariance $K(X_i, X_j)$, the higher-order correlations must fulfill Wick's theorem (also known as Isserlis' theorem) [44, 45],

$$\langle X_1 \cdots X_n \rangle = \begin{cases} 0, & n \text{ odd}, \\ \sum_{\text{Pairings}} \prod_{(i,j)} K(X_i, X_j), & n \text{ even}. \end{cases} \quad (17)$$

Since the sum of the SLTs is strongly non-Gaussian, the higher-order correlations must deviate from the Wick prescription. This is a usual phenomenon observed in field theory and condensed matter physics, in which the integral (or sum) of a stochastic or quantum field over a finite region is shown to deviate from Gaussianity due to the presence of non-Wick higher-order correlations [47–49], which is known as *full-counting statistics*.

Specifically, the conformally invariant case presents a broad interest due to its applicability to critical phenomena [46]. For a 1+1D conformal field theory (CFT), the form of the two-point and the three-point correlators is well known,

$$\langle X_i X_j \rangle \approx \frac{A_2}{|i - j|^{2\Delta}}, \quad (18)$$

$$\langle X_i X_j X_k \rangle \approx \frac{A_3}{|i - j|^{\Delta} |i - k|^{\Delta} |j - k|^{\Delta}}, \quad (19)$$

where Δ is the conformal weight associated to the field, and A_2 and A_3 are constants.

In our case, non-Gaussianity suggests that the three-point correlators should be non-zero. The generic power-law behavior observed within the KPZ class allows us to attempt a CFT Ansatz, even though we do not claim at this stage any conformal invariance in our model. Compliance with the two-point function requires that we use $\Delta = 2/3$. Thus, we hypothesize

$$\langle \bar{t}_i \bar{t}_j \bar{t}_k \rangle \propto \frac{1}{|i-j|^{2/3} |i-k|^{2/3} |j-k|^{2/3}}. \quad (20)$$

Yet, we can perform a sanity check of this expression before advancing further. Does it yield a finite skewness for the arrival times, $\bar{T} = T - \langle T \rangle$? According to our Ansatz, the third moment scales as

$$\langle \bar{T}^3 \rangle = \sum_{ijk} \langle \bar{t}_i \bar{t}_j \bar{t}_k \rangle \sim d^{3-3\Delta}. \quad (21)$$

Indeed, from the definition of the skewness we obtain

$$\gamma_{\bar{T}} = \frac{\langle \bar{T}^3 \rangle}{\langle \bar{T}^2 \rangle^{3/2}} \sim \frac{d^{3-3\Delta}}{(d^{2-2\Delta})^{3/2}} = \text{Const}, \quad (22)$$

so, the Ansatz makes sense. Does it actually work? We show in Fig. 11 the results for two different three-point correlators, for geodesics spanning distance d_{\max} along the diagonal and different LT distributions. Figure 11 (a) shows the decay of $C_3(k) \equiv \langle \bar{t}_i \bar{t}_{i+1} \bar{t}_{i+k} \rangle$ and we check that it agrees with the prediction from Eq. (20),

$$C_3(k) \equiv \langle \bar{t}_i \bar{t}_{i+1} \bar{t}_{i+k} \rangle \sim k^{-2\Delta} = k^{-4/3}. \quad (23)$$

Figure 11 (b) shows the decay of $\hat{C}_3(k) \equiv \langle \bar{t}_i \bar{t}_{i+k} \bar{t}_{i+2k} \rangle$, for which we expect

$$\hat{C}_3(k) \equiv \langle \bar{t}_i \bar{t}_{i+k} \bar{t}_{i+2k} \rangle \sim k^{-3\Delta} = k^{-2}. \quad (24)$$

The faster decay for this type of correlators is harder to capture numerically, yet Fig. 11 (b) manages to catch a glimpse for low values of k .

VI. CONCLUSIONS AND FURTHER WORK

In this work, we have explored the statistical properties of the SLTs, i.e. the link-times *actually selected to form part of different geodesics* in FPP lattices. Naturally, they tend to take lower values than those prescribed by the general LT distribution. Moreover, in similarity to Berkson's paradox, we observe emergent correlations among them induced by the selection procedure, despite the fact that the original LTs are iid random variables.

Specifically, we have considered geodesics –also known as optimal paths– joining points along an axis or along

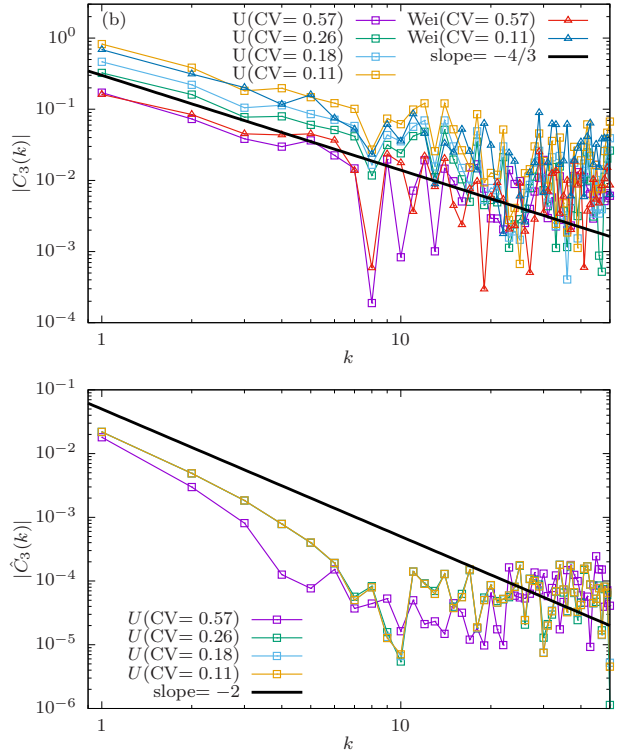


Figure 11. (a) Three-point correlation function $C_3(k)$, defined in Eq. (23), for geodesics reaching d_{\max} along the diagonal and different uniform and Weibull distributions. The solid line represents the predicted $k^{-4/3}$ decay. (b) Alternative three-point correlation function $\hat{C}_3(k)$ defined in Eq. (24), and the theoretically expected k^{-2} decay.

a diagonal of a square lattice, using probability distributions for the LTs in the uniform and Weibull families, for different values of the CV. The SLT probability distribution displays scaling behavior in many regimes. For example, the global mean and deviation of the SLT distribution decay as the distance is increased, approaching a limiting value as a power law with exponent $-2/3$, which we have associated to KPZ behavior. Moreover, geodesics are typically more constrained near their extreme points, and the mean and deviation of the local SLT distribution approach the bulk behavior in a similar fashion. Intriguing directional effects are observed when the geodesic extends along an axis, which require further investigation. Finally, the selection mechanism induces long-range correlations among the SLTs, which decay with their distance along the geodesic as a power-law with exponent $-\gamma = 2\beta - 2 = -4/3$, where $\beta = 1/3$ is the growth exponent of KPZ.

The arrival times in FPP, which are the sums of SLTs, converge to a Tracy-Widom distribution. Therefore the SLTs must violate some of the hypotheses underneath the CLT. We have explored the origin of such violations, and found non-Wick long-range correlations of third order. An Ansatz inspired in conformal symmetry arguments has allowed us to conjecture a scaling form for the three-

point correlation function.

The statistical properties of the SLTs have proved to be far richer than initially expected, and many features deserve further research. For example, in this work we have neglected the effects of the total length of the geodesic. Elucidation of the origin of the TW as a sum of identically distributed but highly correlated SLTs is still incomplete. Indeed, sums of identically distributed but strongly correlated random variables may still be Gaussian if the covariance matrix follows certain regularity constraints, as described in the Breuer-Major theorem, and fall into the different Hermite processes when a non-linear function acts on the variables [44, 45]. Still, this framework does not seem to provide a route to show how the TW distribution may emerge in this context. This question poses an intriguing problem for the mathematical physics com-

munity.

ACKNOWLEDGMENTS

This work has benefited from discussions with R. Cuerno, J.M. López and D. Villarrubia. We acknowledge the Spanish government for financial support through grants PID2021-123969NB-I00, PID2024-159024NB-C21 and PID2024-159024NB-C22, as well as the computational resources and assistance provided by the Centro de Computación de Alto Rendimiento (CCAR-UNED). I.A.D. acknowledges funding from UNED through an FPI scholarship.

[1] I. Karatzas, S.E. Shreve, *Brownian motion and stochastic calculus*, Springer (1988).

[2] H.A. David, H.N. Nagaraja, *Order statistics*, John Wiley & Sons (2003).

[3] J. Berkson, *Limitations of the application of the four-fold table analysis to hospital data*, *Biometrics Bull.* **2**, 47 (1946).

[4] J. Pearl, *The book of why*, Basic Books (2018).

[5] J. de Ron, E.I. Fried, S. Epskamp, *Psychological networks in clinical populations: investigating the consequences of Berkson's bias*, *Psychological Medicine* **51**, 168 (2021).

[6] A.G. Butkevich, A.V. Berdugin, P. Teerikorpi, *Statistical biases in stellar astronomy: the Malmquist bias revisited*, *Mon. Not. R. Astron. Soc.* **362**, 321 (2005).

[7] R.L. Prentice, J.D. Klabfleisch, A.V. Peterson Jr, N. Flournoy, V.T. Farewell, N.E. Breslow, *The analysis of failure times in the presence of competing risks*, *Biometrics* **34**, 541 (1978).

[8] M.G. Bulmer, *The effect of selection on genetic variability*, *The American Naturalist* **105**, 201 (1971).

[9] S. Havlin, L.A. Braunstein, S.V. Buldyrev, R. Cohen, T. Kalisky, S. Sreenivasan, H.E. Stanley, *Optimal path in random networks with disorder: A mini review*, *Physica A* **346**, 82 (2005).

[10] P. Bhattacharyya, A. Chatterjee, *Geometric properties of optimal and most probable paths on randomly disordered lattices*, in *Statistics of Linear Polymers in Disordered Media*, p. 271, edited by E. Bikas, K. Chakrabarti, Elsevier (2005).

[11] J.M. Hammersley, D.J.A. Welsh, *First-passage percolation, subadditive processes, stochastic networks and generalized renewal theory*, in *Bernoulli, Bayes, Laplace Anniversary Volume*, p. 61, edited by J. Neyman, L.M. LeCam, Springer (1965).

[12] A. Auffinger, M. Damron, J. Hanson, *50 Years of FPP*, University Lecture Series Vol. 68 (American Mathematical Society, 2017).

[13] S.N. Santalla, J. Rodríguez-Laguna, T. LaGatta, R. Cuerno, *Random geometry and the Kardar-Parisi-Zhang universality class*, *New J. Phys.* **17**, 033018 (2015).

[14] S.N. Santalla, J. Rodríguez-Laguna, A. Celi, R. Cuerno, *Topology and the Kardar-Parisi-Zhang universality class*, *J. Stat. Mech.* 023201 (2017).

[15] R. Dobrin, P.M. Duxbury, *Minimum spanning trees on random networks*, *Phys. Rev. Lett.* **86**, 5076 (2001).

[16] P. van Mieghem, S.M. Magdalena, *Phase transition in the link weight structure of network*, *Phys. Rev. E* **72**, 056138 (2005).

[17] P. van Mieghem, S. van Langen, *Influence of the link weight structure on the shortest path*, *Phys. Rev. E* **71**, 056113 (2005).

[18] Z. Wu, L.A. Braunstein, S. Havlin, H.E. Stanley, *Transport in weighted networks: Partition into superhigh-ways and roads*, *Phys. Rev. Lett.* **96**, 148702 (2006).

[19] H. Wang, J.M. Hernandez, P. van Mieghem, *Betweenness centrality in a weighted network*, *Phys. Rev. E* **77**, 046105 (2008).

[20] T. Halpin-Healy, Y.-C. Zhang, *Kinetic roughening phenomena, stochastic growth, directed polymers and all that*, *Phys. Rep.* **254**, 215 (1995).

[21] E. López, L.A. Braunstein, *Disorder-induced limited path percolation*, *Europhys. Lett.* **97**, 66001 (2012).

[22] B. Fortz, M. Thorup, *Optimizing OSPF/IS-IS weights in a changing world*, *IEEE J. Sel. Areas Commun.* **20**, 756 (2002).

[23] R. Mahajan, N. Spring, D. Wetherall, T. Anderson, *Inferring link weights using end-to-end measurements*, *Proc. IMW'02 Marseille*, p. 231, ACM (2002).

[24] A.-L. Barabási, *Invasion percolation and global optimization*, *Phys. Rev. Lett.* **76**, 3750 (1996).

[25] M. Cieplak, A. Maritan, J.R. Banavar, *Invasion percolation and Eden growth: Geometry and universality*, *Phys. Rev. Lett.* **76**, 3754 (1996).

[26] M. Porto, S. Havlin, S. Schwarzer, A. Bunde, *Optimal path in strong disorder and shortest path in invasion percolation with trapping*, *Phys. Rev. Lett.* **79**, 4060 (1997).

[27] J.S. Andrade, S.V. Buldyrev, N.V. Dokholyan, S. Havlin, P.R. King, Y.K. Lee, G. Paul, H.E. Stanley, *Flow between two sites on a percolation cluster*, *Phys. Rev. E* **62**, 8270 (2000).

[28] E. López, S.V. Buldyrev, L.A. Braunstein, S. Havlin, H.E. Stanley, *Possible connection between the optimal path and flow in percolation clusters*, *Phys. Rev. E* **72**, 056131 (2005).

- [29] Z. Wu, E. López, S.V. Buldyrev, L.A. Braunstein, S. Havlin, H.E. Stanley, *Current flow in random resistor networks: The role of percolation in weak and strong disorder*, Phys. Rev. E **71**, 045101(R) (2005).
- [30] G. Li, L.A. Braunstein, S.V. Buldyrev, S. Havlin, H.E. Stanley, *Transport and percolation theory in weighted networks*, Phys. Rev. E **75**, 045103(R) (2007).
- [31] Y.M. Strelniker, R. Berkovits, A. Frydman, S. Havlin, *Percolation transition in a two-dimensional system of Ni granular ferromagnets*, Phys. Rev. E **69**, 065105(R) (2004).
- [32] Y.M. Strelniker, S. Havlin, R. Berkovits, A. Frydman, *Hopping percolation transition in granular ferromagnets*, J. Appl. Phys. **99**, 08P905 (2006).
- [33] D. Tolić, K.-K. Kleineberg, N. Antulov-Fantulin, *Simulating SIR processes on networks using weighted shortest paths*, Sci. Rep. **8**, 6562 (2018).
- [34] J.S. Andrade, E.A. Oliveira, A.A. Moreira, H.J. Herrmann, *Fracturing the optimal paths*, Phys. Rev. Lett. **103**, 225503 (2009).
- [35] D. Villarrubia-Moreno, P. Córdoba-Torres, *Unified scaling for the optimal path length in disordered lattices*, Phys. Rev. E **109**, 054114 (2024).
- [36] P. Córdoba-Torres, S.N. Santalla, R. Cuerno, J. Rodríguez-Laguna, *Kardar-Parisi-Zhang universality in first passage percolation: The role of geodesic degeneracy*, J. Stat. Mech. 063212 (2018).
- [37] I. Álvarez Domenech, J. Rodríguez-Laguna, R. Cuerno, P. Córdoba-Torres, S.N. Santalla, *Shape effects in the fluctuations of random isochrones on a square lattice*, Phys. Rev. E **109**, 034104 (2024).
- [38] M. Kardar, G. Parisi, Y.C. Zhang, *Dynamic scaling of growing interfaces*, Phys. Rev. Lett. **56**, 889 (1986).
- [39] A.-L. Barabási, H. E. Stanley, *Fractal Concepts in Surface Growth* Cambridge University Press (1995).
- [40] T. Halpin-Healy and K.A. Takeuchi, *A KPZ cocktail-shaken, not stirred... Toasting 30 years of kinetically roughened surfaces*, J. Stat. Phys. **160**, 794 (2015).
- [41] W. Feller, *An introduction to probability theory and its applications, vol. II*, John Wiley & Sons (1968).
- [42] I.A. Ibragimov, Yu.V. Linnik, *Independent and stationary sequences of random variables*, Wolters-Noordhoff Publ. (1971).
- [43] P. Billingsley, *Probability and measure*, John Wiley & Sons (1995).
- [44] G. Peccati, M.S. Taqqu, *Wiener chaos: moments, cumulants and diagrams*, Bocconi Univ. Press & Springer (2011).
- [45] V. Pipiras, M.S. Taqqu, *Long range dependence and self-similarity*, Cambridge University Press (2017).
- [46] P. di Francesco, P. Mathieu, D. Sénéchal, *Conformal Field Theory*, Springer (1997).
- [47] C.J. Fewster, S. Hollands, *Probability distributions for the stress tensor in conformal field theories*, Lett. Math. Phys. **109**, 747 (2018).
- [48] F. Camia, C. Garban, C.M. Newman, *Planar Ising magnetization field I. Uniqueness of the critical scaling limit*, Ann. Prob. **43**, 528 (2015).
- [49] M.C. Anthony, C.J. Fewster, *Explicit examples of probability distributions for the energy density in two-dimensional conformal field theory*, Phys. Rev. D **101**, 025010 (2020).
- [50] J.T. Cox, R. Durrett, *Some limit theorems for percolation processes with necessary and sufficient conditions*, Ann. Probab., **9**, 583, (1981).
- [51] M. Damron, *Random growth models: shape and convergence rate*, ArXiv:1804.05716 (2018).
- [52] J.A. Domínguez-Molina, *The Tracy-Widom distribution is not infinitely divisible*, ArXiv:1601.02898 (2016).